13 Superconductivity and Magnetism

M. Bendele (till May 2012), S. Bosma, Z. Guguchia, L. Howald, H. Keller, A. Maisuradze, S. Siegrist, E. Stilp, and S. Weyeneth

Visiting scientists: M. V. Eremin, B. I. Kochelaev, R. Puzniak, and A. Shengelaya
Emeritus members: M. Mali, K. A. Müller, J. Roos, and T. Schneider

in collaboration with:
Bayerische Akademie der Wissenschaften Garching, (A. Erb), Brookhaven National Laboratory (I. Bozovic, A. Gozar), Commissariat à l'énergie atomique Grenoble (G. Lapertot, P. Dalmas de Réotier, A. Yaouanc), EPFL Lausanne (H. Berger, D. Pavuna), ETH Zürich (J. Karpinski, N. D. Zhigadlo), Leibniz-Institut für Festkörper- und Werkstoffforschung Dresden (R. Hühne, P. Pahlke), Kazan State University (M. V. Eremin, B. I. Kochelaev), Max Planck Institute Stuttgart (A. Bussmann-Holder, J. Köhler, G. Logvenov), Paul Scherrer Institute (K. Conder, R. Khasanov, E. Morenzoni, A. Suter), Polish Academy of Sciences (R. Puzniak), Tbilisi State University (A. Shengelaya), University of British Columbia, Canada (R.F. Kiefl, W. Hardy)

We report recent results of active research projects in the field of unconventional superconductors, magnetism and magneto-electric materials. Different experimental techniques were combined for our studies, including muon-spin rotation (μSR), torque magnetometry, electron paramagnetic resonance (EPR), and standard characterization probes (specific heat, superconducting quantum interference device (SQUID) magnetometry and resistivity). Several experiments were performed under hydrostatic pressure (0-8 GPa).

In the first section the coupling between spins and phonons in $EuTiO_3$ was observed to occur at temperatures far above the onset of the magnetic order. In Cu_2OSeO_3 the magneto-electric properties were studied using an electric field modulated ferromagnetic resonance technique recently internally developed. μSR experiments revealed a strong variation of the number of superconducting pairs under pressure in the heavy fermions superconductor $CeCoIn_5$. The magnetic phase diagram of thin films of the high-temperature cuprate superconductor (HTC) $La_{2-x}Sr_xCuO_4$ was established by means the low energy μSR technique. Finally, an unusual *lock-in* effect was found in the HTC $YBa_2Cu_3O_{7-\delta}$ by torque magnetometry.

13.1 Magnetic field enhanced structural instability in $EuTiO_3$

Multi-functional systems with properties that can be tuned by different external sources have attracted attention for many years. The focus in this research field is mainly on multiferroics where a magnetic field modifies the dielectric properties, and an electric field may influence the magnetic characteristics.

In the search for novel multiferroic materials, the work of Katsufuji and Takagi [1] on the perovskite $EuTiO_3$ (ETO) has recently invoked hopes of having a new compound with the desired properties. It was demonstrated that the dielectric constant of ETO shows a dramatic decrease upon the onset of the anti-ferromagnetic (AFM) phase transition at $T_N = 5.5$ K. This unexpected behaviour clearly demonstrates that a strong spin-lattice coupling is present in the system. In addition to the observed low-T AFM phase, very recent experimental and theoretical studies have revealed the presence of a structural phase transition in ETO at $T_s = 282$ K [2–4]. This structural phase transition has been suggested to be caused by the oxygen octahedral tilting instability as in $SrTiO_3$ (STO) [5]. However, in STO the transition is observed at much lower temperature $T_s = 105$ K.

Recently, we have investigated magnetic field effects on the structural instability of ETO at $T_S = 282$ K [6]. The motivation for these experiments stems from our previous observation of the existence of a damped muon spin rotation (μSR) decay rate λ_{para} at temperatures far above T_N, which follows closely the temperature dependence of the transverse acoustic zone boundary mode [4]. This finding suggests that a strong paramagnon-phonon coupling exists far above T_N. We identify the structural phase transition temperature by specific heat measurements and perform these measurements under an applied magnetic field [6].

At high temperatures the anomaly stemming from the structural phase transition is visible as a distinct peak (Fig. 13.1). T_S increases non-linearly with magnetic field [6]. The substantial increase of T_S with magnetic field indicates a strong spin-phonon coupling at temperatures

far above the actual magnetic order. This interaction between the applied magnetic field and the crystallographic structure may provide a new path towards the realisation of multi-functionality in complex perovskite lattices by tuning dielectric, piezoelectric, and magnetoelectric couplings.

[1] T. Katsufuji and H. Takagi, Phys. Rev. B **64**, 054415 (2001).

[2] A. Bussmann-Holder *et al.*, Phys. Rev. B **83**, 212102 (2011).

[3] Z. Guguchia *et al.*, Phys. Rev. B **85**, 134113 (2012).

[4] A. Bussmann-Holder *et al.*, New J. Phys. **14**, 093013 (2012).

[5] K. A. Müller *et al.*, Phys. Rev. B **19**, 3593 (1979).

[6] Z. Guguchia *et al.*, J. Phys.: Condens. Matter **24**, 492201 (2012).

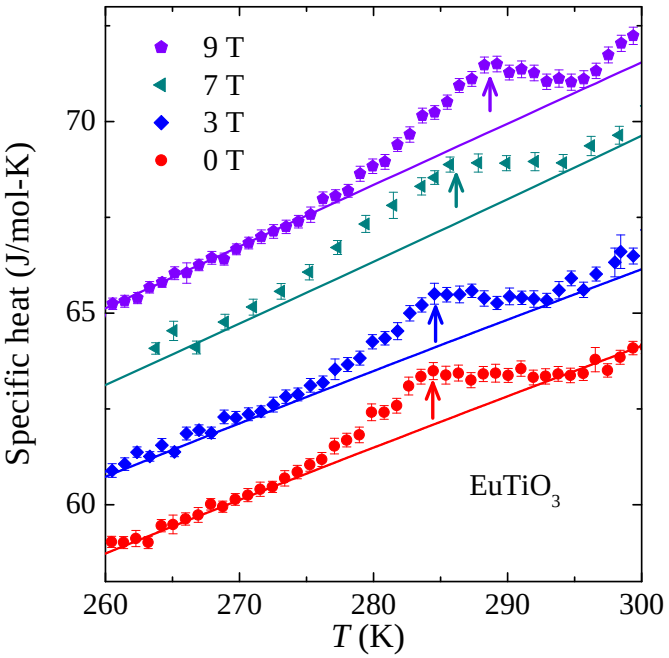

FIG. 13.1 – The specific heat of $EuTiO_3$ as a function of temperature within a limited temperature regime around the structural phase transition temperature T_S for fields of 0, 3, 7, and 9 T. For clarity the data are shifted by $2 Jmol^{-1}K^{-1}$ relative to each other with increasing magnetic field [6].

13.2 Magneto-electric effect on spin-wave resonances in Cu_2OSeO_3

Magneto-electric (ME) materials, exhibiting coupled and microscopically coexisting magnetic and electric polarizations, have attracted considerable interest in recent years [1, 2]. This coupling allows one to influence the magnetic state of a ME material via an external electric field, thus opening a broad range of possible technical applications of such materials.

In collaboration with the EPFL we investigated magnetic and magneto-electric properties of Cu_2OSeO_3 by means of the novel electric field modulated (EFM) ferromagnetic resonance (FMR) technique [3]. In standard FMR or spin-wave resonance (SWR) experiments a resonant absorption of microwave radiation by a Zeeman-split spin system is observed. In order to increase the sensitivity of FMR a lock-in detection method is used. A reference frequency of the lock-in detector is used for a weak quasi-static modulation of the Zeeman splitting, *e.g.* by magnetic field modulation (MFM) of the applied field. This leads to a weak modulation of the absorbed microwave power signal which is supplied to the input of a lock-in amplifier. As a result the lock-in detected signal is proportional to the amplitude of MFM and vanishes when there is no modulation of the Zeeman splitting. The situation is different for ME materials where the Zeeman splitting can also be modulated by an applied electric field. Due to ME coupling EFM leads to microscopic MFM proportional to the ME coupling strength. This modulation is present only in magneto-electrics and allows one to detect selectively FMR and SWR of ME materials. Thus, FMR with EFM

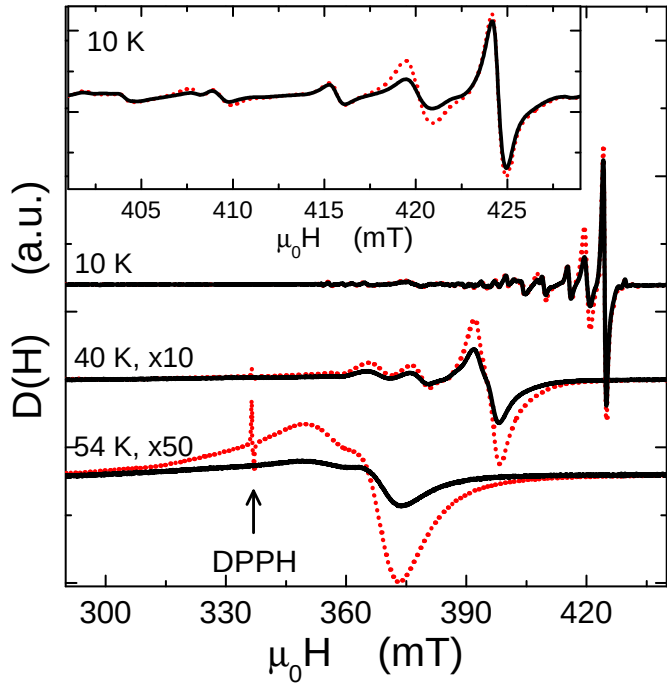

FIG. 13.2 – Temperature dependence of SWR signals of single-crystal Cu_2OSeO_3 detected using the MFM technique (dotted line) and the EFM technique (solid line). The sharp peak visible at 340 mT and 54 K is the signal of the marker sample DPPH which is present only in the case of MFM. The inset shows the expanded spectra at 10 K around 415 mT.

can serve as a sensitive microscopic tool for investigation of ME phenomena.

We applied this technique for investigating the ferrimagnetically ordered Cu^{2+} spin system in Cu_2OSeO_3 [3]. In Fig. 13.2 we show the results of FMR experiments using MFM and EFM techniques. While ME Cu_2OSeO_3 induces a SWR signal for both MFM and EFM, the paramagnetic resonance signal of $C_{18}H_{12}N_5O_6$ (DPPH) is present only for MFM. We observed for the first time series of SWR signals induced via ME coupling. An external electric field **E** induces a magnetic field component $\mu_0 H^i = \gamma E$ along the applied magnetic field **H** with $\gamma = 0.7(1)$ μT/(V/mm) at 10 K consistent with our previous μSR studies [4]. Temperature and angular dependencies of $\alpha = \gamma/C$ ($C = 1.76$ μT·mm·V^{-1} a calibration constant) are shown in Fig. 13.3. $\gamma(T)$ nearly follows that of the spin susceptibility J^{M} and rapidly decreases above the Curie temperature $T_{\mathrm{c}} = 57$ K [3]. The ratio $\langle\alpha\rangle/J^{\mathrm{M}}$ varies slowly with temperature and shows no anomaly at T_{c}, suggesting that ME effect is not related to the long range magnetic order.

[1] N. A. Spaldin and M. Fiebig, Science **309**, 391 (2005).

[2] M. Fiebig, J. Phys D: Appl. Phys. **38**, R123 (2005).

[3] A. Maisuradze *et al.*, Phys. Rev. Lett. **108**, 247211 (2012).

[4] A. Maisuradze *et al.*, Phys. Rev. B **84**, 064433 (2011).

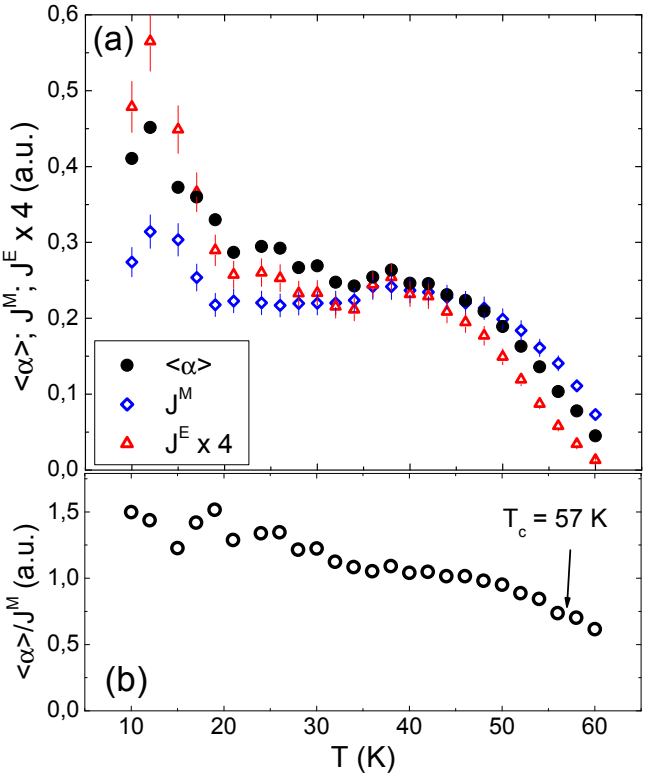

FIG. 13.3 – (a) Temperature dependence of the average ME effect parameter $\langle\alpha\rangle$ and the signal intensities J^E and J^M of Cu_2OSeO_3 detected by EFM and MFM, respectively. (b) Temperature dependence of the ratio $\langle\alpha\rangle/J^M$ showing no anomaly at $T_{\mathrm{c}} = 57$ K.

13.3 Strong reduction of the magnetic penetration depth in $CeCoIn_5$ under pressure

In the tetragonal heavy fermion system $CeCoIn_5$ the unconventional superconducting state was probed by means of transverse field muon spin rotation (TF μSR) [1]. In a μSR experiment the muons act as highly sensitive local probe of the magnetic field. TF μSR experiments were performed above and below the superconducting transition temperature (T_{c}) in single crystals of $CeCoIn_5$ under pressure. An example of the obtained magnetic field profiles is shown in inset of Fig. 13.4. Above T_{c} (black squares) the mean magnetic field corresponds to the applied value and the magnetic field distribution is due to the nuclear moments. Below T_{c} (red circles) the mean value of the magnetic field is reduced due to diamagnetism and the field distribution is asymmetric. The asymmetry arises from an additional contribution to the field distribution generated by the vortex lattice (pink area represents half of the vortex lattice contribution) which is uniquely determined by the value of the magnetic penetration depth (λ).

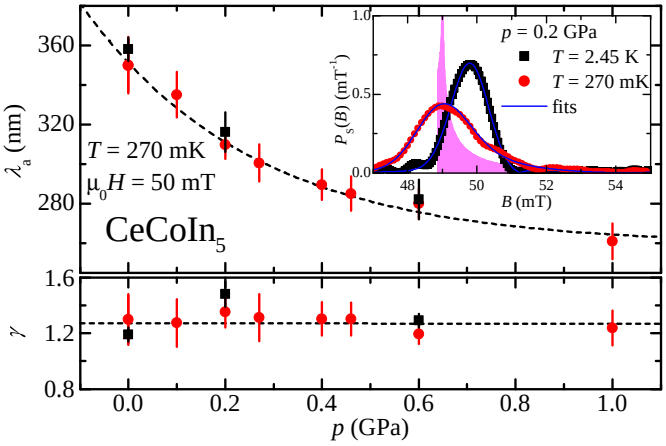

FIG. 13.4 – Pressure dependence of the in-plane magnetic penetration depth (λ_a) and the penetration depth anisotropy ($\gamma = \lambda_c/\lambda_a$). In the inset a typical field distribution probed by μSR is shown.

Using the field distribution probed by μSR, the pressure dependence ($0 - 1$ GPa) of the basal-plane magnetic penetration depth (λ_a), the penetration depth anisotropy

($\gamma = \lambda_c/\lambda_a$), and the temperature dependence of $1/\lambda_i^2$ ($i = a, c$) was studied. A strong decrease of λ_a with pressure was observed, while γ is pressure independent (Fig. 13.4). Furthermore, no significant variations in $\lambda_i^2(0)/\lambda_i^2(T)$ with pressure were obtained. A linear relationship between $1/\lambda_a^2(270\text{mK})$ and T_c was also found. Within the London model the large decrease of λ_a with pressure indicates an increase of the number of superconducting quasi-particles by a factor of about 2. This increase is probably related with the presence of a quantum critical point in this pressure range.

[1] L. Howald *et al.*,
Phys. Rev. Lett. **110**, 017005 (2013).

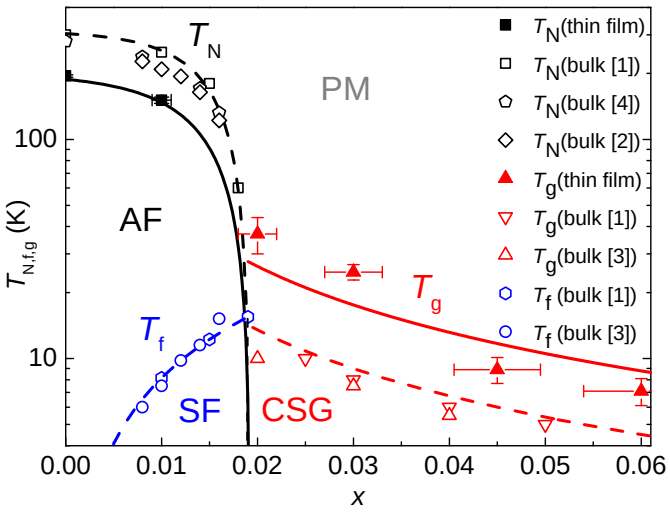

FIG. 13.5 – Magnetic phase diagram of LSCO for thin film samples (solid lines) and bulk material (dashed lines). Néel temperatures T_N, freezing temperatures T_f and glass transition temperatures T_g are shown in dependence of the Sr content x [1–4]. The black lines are guides to the eye, the blue and red lines follow the relations $T_f \propto x$ and $T_g \propto 1/x$.

13.4 Thin film phase diagram of $La_{2-x}Sr_xCuO_4$

Thin-film studies open the door to new physics, since the properties of thin-film materials can be tailored which is difficult or even impossible for bulk samples. The magnetic phase diagram of $La_{2-x}Sr_xCuO_4$ (LSCO) thin films was intensively studied. The samples used are MBE grown and have a thickness of 53 nm. They cover a doping range of $x = 0.00 - 0.06$. XRD and resistivity measurements confirm that the c axis of LSCO thin films depends linearly on the doping level x, as in the bulk case. The resistance is higher at low x compared to bulk samples and decreases with increasing x over two decades.

To study the magnetic phase diagram more in detail, low energy muon spin rotation (LE-μSR) measurements were performed. Muon energies in the range $1 - 30$ keV allow to investigate thin film samples, because muons stop on a nano-meter scale in condensed matter. From weak transverse magnetic field (wTF) μSR measurements magnetic transition temperatures as well as magnetic volume fractions were determined. From measurements without an applied magnetic field the internal magnetic field B_{loc} present at the muon stopping site was identified.

The phase diagram of LSCO consists of several regimes as shown in Fig. 13.5: the high temperature paramagnetic (PM) phase, the anti-ferromagnetic (AF) dome, the low temperature spin freezing (SF) region, and the *cluster spin glass* (CSG) phase. The PM phase is present for all doping levels at higher temperatures. In the AF phase ($x < 0.02$) static moments are present which lead to oscillations in the μSR time spectra. The Néel temperatures T_N of the thin film samples determined from wTF-μSR measurements are reduced compared to those of bulk material (Fig. 13.5). At low temperatures a freezing of the additional charge carriers is expected from bulk measurements for $x > 0.00$ (SF phase). The temperature dependence of B_{loc} shows instead no increase of the slope dB_{loc}/dT at low temperatures T. This implies that no spin freezing is observed down to 5 K. Surprisingly, for $x = 0.00$ two local magnetic fields of $B_{loc,1}(0\text{ K}) = 40.9(4)$ mT and $B_{loc,2}(0\text{ K}) = 11.2(1)$ mT were detected at the muon stopping site in zero field measurements in the AF phase. In bulk only one local magnetic field of $B_{loc}(0\text{ K}) = 43$ mT is reported [4]. This difference could arise from changes in the spin arrangement of copper electronic magnetic moments. In the so called *cluster spin glas* phase ($x \geq 0.02$) dynamical spin and charge stripes are present in cuprate systems due to micro-segregation of mobile holes. AF hole-poor areas are separated by non-magnetic hole-rich domain walls. At low temperatures the dynamics of the stripes slow down and oscillations are observed in the LE-μSR zero field asymmetry time spectra. The determined glass transition temperatures T_g are all well above the bulk values. Strain induced changes of the higher order magnetic coupling constants as well as oxygen off-stoichiometry are unlikely to explain the observed differences to bulk. It is concluded that strain induced disorder is probable the main reason of the observed differences to bulk. The magnetic phase diagram was determined for LSCO thin films, is a base for future studies of multi-layer and super-lattices.

[1] Ch. Niedermayer *et al.*,
Phys. Rev. Lett. **80**, 3843 (1998).

[2] J. H. Cho *et al.*,
Phys. Rev. Lett. **70**, 222 (1993).

[3] F. C. Chou *et al.*,
Phys. Rev. Lett. **71**, 2323-2326 (1993).

[4] F. Borsa *et al.*,
Phys. Rev. B **52**, 7334 (1995).

13.5 Vortex lock-in transition in $YBa_2Cu_3O_{7-\delta}$

In low anisotropy superconductors, a three-dimensional (3D) to two-dimensional (2D) crossover can take place when the superconducting coherence length along the *c*-axis becomes smaller than the distance between the planes supporting superconductivity. For $YBa_2Cu_3O_{7-\delta}$, this happens at $T_{cr} \simeq 76$ K.

When the applied magnetic field direction is nearly parallel to the *ab*-plane, a lock-in transition of the vortices may take place [1]. In this case, the vortex is confined between the superconducting layers, even if the field is not aligned with these layers. This minimizes superconducting condensation energy at the cost of magnetic energy coming from the misalignment of vortices and field, since the cores do not cross the layers anymore. The lock-in was observed mainly in high anisotropy materials, but also in $YBa_2Cu_3O_{7-\delta}$ and other layered superconductors. $YBa_2Cu_3O_{7-\delta}$ is of particular interest for lock-in studies, since its low anisotropy allows one to observe the onset of lock-in far below T_c, where critical fluctuations make the analysis difficult. The theoretical models for lock-in which are relevant for $YBa_2Cu_3O_{7-\delta}$ are presented in [2] and [3].

We performed angular torque measurement on clean detwinned $YBa_2Cu_3O_{7-\delta}$ single crystals [4]. A simple geometric calculation of the torque in the locked-in regime yields a linear torque dependence on the angle θ between the applied field H and the crystallographic *c*-axis. The measured shape of the torque as a function of θ is the same as predicted in [2], although this model was originally developed for quasi-2D superconductors. Figure 13.6 shows the torque in the lock-in region. The lock-in angle θ_{lock} is the point at which the torque ceases to follow the linear dependence observed around the *ab*-plane, corresponding to the locked-in state. θ_{lock} is smaller at low temperatures, as expected for a pinning-like effect. Surprisingly, it also is smaller at high fields. The lock-in should happen when the perpendicular component of the field $H^{||c}$ goes below $H_{c1}^{||c}$. Field penetration across the layers is then impossible, thus locking the vortices between the planes. In this model, $\pi/2 - \theta_{lock}$ is inversely proportional to H, as observed in high-anisotropy cuprates.

Torque data present an angular irreversibility between the clockwise (CW) and counter-clockwise (CCW) branches, which is usually due to pinning and

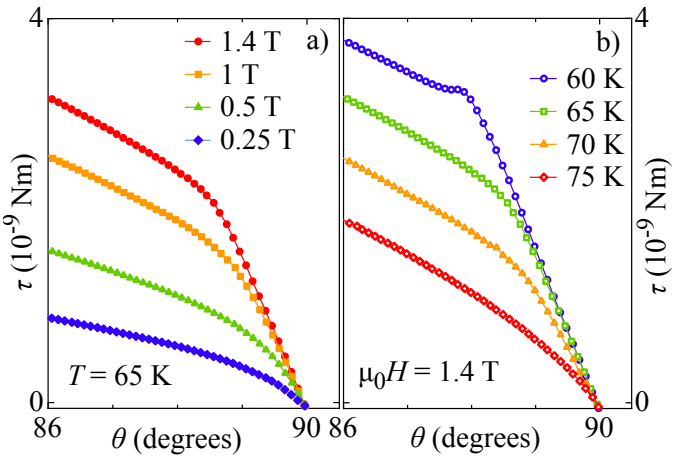

FIG. 13.6 – a) Torque of detwinned single crystal $YBa_2Cu_3O_{7-\delta}$ as a function of angle θ for various fields at 65 K. b) $\tau(\theta)$ for various temperatures at 1.4 T.

can be reduced by the shaking technique [5]. The difference between the 3D London prediction and the CW-CCW averaged torque, which is interpreted as lock-in, is too large to be an artifact of irreversibility. The shaking efficiency limit is reached when a small peak appears at the limit of the lock-in domain; in our case this happens at low temperature and high fields. This peak usually masks the lock-in effect in lower quality crystals.

The lock-in angle θ_{lock} can also be defined as the angle where the torque slope diverges from the *ab*-plane value. With this definition, θ_{lock} still increases at low temperatures and at high fields. This could be due to the fact that θ_{lock} becomes more difficult to identify at higher temperatures and lower fields due to the increased curvature of the graph. However, the simple model of θ_{lock} is not observed in $La_{2-x}Sr_xCuO_4$ [6]. It is thus possible that the 1/H model holds only for high-anisotropy superconductors.

[1] D. Feinberg and C. Villard,
Phys. Rev. Lett. **65**, 919 (1990).

[2] D. Feinberg and A. M. Ettouhami,
Int. J. Mod. Phys. B **7**, 2085 (1993).

[3] L. N. Bulaevskii, Phys. Rev. B **44**, 910 (1991).

[4] S. Bosma *et al.* , Phys. Rev. B **86**, 174502 (2012).

[5] M. Willemin *et al.* , Phys. Rev. B **58**, R5940 (1998).

[6] V. Vulcanescu *et al.* , Phys. Rev. B **50**, 4139 (1994).